Patterning of Plasmonic Nanoparticles into Multiplexed One-Dimensional Arrays Based on Spatially Modulated Electrostatic Potential

Lin Jiang,[†] Yinghui Sun,[†] Christoph Nowak,[†,§] Asmorom Kibrom,[§] Changji Zou,[†] Jan Ma,[†] Harald Fuchs,[‡] Shuzhou Li,[†,*] Lifeng Chi,[‡,*] and Xiaodong Chen[†,*]

[†]School of Materials Science and Engineering and the Center for the Biomimetic Sensor Sciences, Nanyang Technological University, 50 Nanyang Avenue, 639798 Singapore, [‡]Physikalisches Institut, Westfaelische Wilhelms-Universitaet Muenster, and Center for Nanotechnology (CeNTech), Muenster, 48149 Germany, and [§]Austrian Institute of Technology GmbH—AIT, Donau-City Str. 1, Vienna, 1220 Austria

ABSTRACT We report a new strategy to pattern plasmonic nanoparticles into multiplexed one-dimensional arrays based on the spatially modulated electrostatic potential. The 32 nm Au nanoparticles can be simultaneously deposited on one chip with tunable interparticle distance by solely adjusting the width of the grooves. Furthermore, 32 and 13 nm Au nanoparticles can be selectively deposited in grooves of different widths on one chip. As a result, the surface plasmon absorption bands on the chip can be tuned depending on the interparticle distance or the particle size of multiplex 1D arrays, which could enhance the Raman scattering cross section of the adsorbed molecules and result in multiplex surface-enhanced Raman scattering (SERS) response on the chip. This strategy provides a general method to fabricate 1D multiplex arrays with different particle sizes and interparticle distances on one chip.

KEYWORDS: spatially modulated electrostatic potential · multiplexed one-dimensional arrays · plasmonic nanoparticle · patterning · surface-enhanced Raman scattering

Developing active plasmonic devices based on metal nanoparticles is drawing much attention recently due to their promising applications, such as biosensing,[1] optoelectronics,[2] and optical antennas.[3] Methods to integrate plasmonic nanoparticles into functional devices are commonly summarized as "top-down" and "bottom-up". In the top-down approach, the features are written directly or transferred onto a substrate, for example, by optical and e-beam lithography, and then the plasmonic nanostructures are engraved by applying appropriate etching and deposition processes. Although the features of plasmonic structures could go down to sub-20 nm, the limitation arises from the low efficiency on patterning small features over a large area, which is a prerequisite for practical applications.[4] Alternatively, various bottom-up methods, such as interfacial self-assembly[5,6] and template-directed assembly,[7] have received considerable attention in assembling plasmonic nanoparticles into organized structures based on the significant progress in the synthesis of nanoparticles with desired size and shape.[8−10]

Among various configurations, one-dimensional (1D) nanoparticle arrays are of particular interest because they can serve as ideal platforms for developing nanoscale devices with cooperative properties, such as surface plasmon resonance, single electron transport, and waveguiding.[11−15] Template-assisted assembly is a common method to construct 1D arrangements of nanoparticles,[4,16−20] where a linear topographic structure defined by lithography is used to trap the nanoparticles into defined positions. The geometric parameters, such as width and length, of the templates play key roles for the nanoparticle arrangement.[21−25] The concepts of self-assembly based on the intrinsic magnetic or electric dipoles of nanoparticles, dewetting, or solvent evaporation provide alternative ways to realize 1D nanoparticle alignment.[6,26−28] However, these strategies can only produce the same sized particle lines on the same substrate with a defined particle distance. It remains a challenge to fabricate 1D nanoparticle arrays with tunable interparticle distance or 1D nanoparticle arrays with different particle size on the same substrate. Such multiplexed 1D nanoparticle arrays would be interesting for the investigation of their collective physical properties, such as surface plasmon resonance and waveguiding, which strongly depend on the particle size, spacing, and higher-order structures.[5,29,30] In addition, such multiplexed arrays are a

* Address correspondence to chenxd@ntu.edu.sg, chi@uni-muenster.de, lisz@ntu.edu.sg.

Received for review August 4, 2011 and accepted September 3, 2011.

Published online September 03, 2011
10.1021/nn202967f

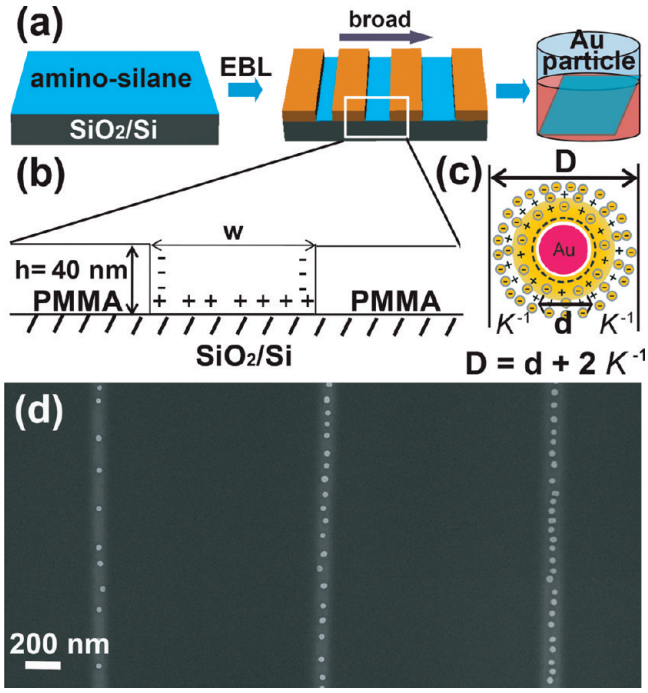

Figure 1. (a) Schematic illustration of the deposition of Au nanoparticles into the 1D grooves defined by EBL. (b) Cross section of the 1D groove with positively charged silicon substrate surface and negatively charged profile of PMMA layer. (c) Effective diameter (*D*) of a Au nanoparticle determined by the diameter of the rigid core (*d*) and the thickness of the double charge layers (K^{-1}). (d) SEM image of single-particle chains with tunable interparticle distance (center to center, from 56 ± 5, 76 ± 5, to 152 ± 10 nm) depending on the groove width (110, 90, and 65 nm, respectively) on the same chip.

kind of encoded nanostructures, which have potential applications in computation, brand protection, disease diagnostics, drug screening, and environmental analysis.[10,31,32]

Herein, we report a new strategy to pattern the plasmonic nanoparticles into multiplexed 1D arrays based on spatially modulated electrostatic potential. Previously, charged nanoparticles have been selectively assembled onto the chemically functionalized substrate surface through electrostatic interaction.[20,33,34] Our strategy is a synergetic combination of geometry-mediated trapping with electrostatic interaction between nanoparticles and surface to produce spatially modulated electrostatic potential. Multiplexed 1D nanoparticle arrays with tunable interparticle distance or multiplexed 1D nanoparticle arrays with different particle size on the same substrate are demonstrated. As proof-of-concept, we demonstrate a multiplexed surface-enhanced Raman scattering (SERS) response on such patterned structures since the surface plasmon absorption bands can be tuned depending on the interparticle distance or the particle size.

RESULTS AND DISCUSSION

In a typical experiment, as sketched in Figure 1a, the silicon substrate surface was first functionalized with a monolayer of aminopropyltriethoxysilane (APTES), which provided positively charged amine groups (+35 ± 3 mV; ζ-potential). Then a poly(methyl methacrylate) (PMMA) layer (40 nm thickness) was spin-coated onto the surface, and the 1D groove template with different widths (65, 90, and 110 nm) were defined by electron-beam lithography (EBL). It is important to note that the profile of the generated 1D grooves was negatively charged by e-beam irradiation (Figure 1b).[35,36] Finally, the 1D groove patterned substrate was immersed into the 32 nm citrate-stabilized Au nanoparticle (−38 ± 5 mV; ζ-potential) solution (>10 h), where the ionic strength *I* of the Au nanoparticle solution was about 5.0×10^{-4} mol/L. In the solution, the effective diameter (*D*) of the nanoparticles is determined by the diameter of the rigid core (*d*) and the thickness of the double charge layers (1/*K*) (Figure 1c).[20] Herein, since $K = 3.288\sqrt{I}$, the calculated thickness of the double layer is about 13.6 nm, resulting in an effective diameter of about 59 nm for 32 nm Au nanoparticles. In order to have 1D single-particle arrays, one must make sure that the effective diameter of the particle is smaller than the groove width.[20] Therefore, we rationally designed a 1D groove pattern with different groove widths ranging from 65 to 110 nm, which were large enough to host the Au nanoparticles. It was found that the 32 nm Au nanoparticles can form well-aligned 1D single-particle chains in these 1D grooves (Figure 1d). Furthermore, the average interparticle distance between two adjacent Au nanoparticles increased from 56 ± 5, 76 ± 5, to 152 ± 10 nm, with the groove width decreasing from 110, 90, to 65 nm, respectively. This result showcases that we can get multiplexed 1D nanoparticle arrays

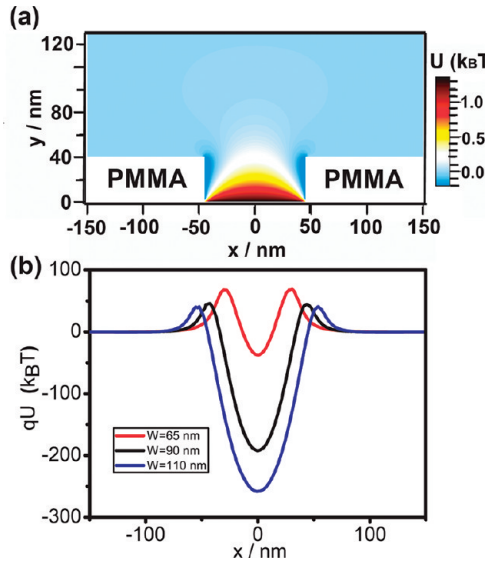

Figure 2. (a) Two-dimensional electrostatic potential distribution obtained by solving the Poisson−Boltzmann equation. (b) Electrostatic energy of a point charge of q ($-38e$) as a function of x along a contour of $y = -50$ nm and the effect of channel width on the electrostatic potential distribution.

with tunable interparticle distance on the same substrate just by modulating the groove width.

To interpret the above result, we have calculated the electrostatic potential distribution in a single groove by numerically solving the two-dimensional Poisson−Boltzmann equation:[37,38]

$$\Delta U = (\kappa a)^2 \sinh(U) \quad (1)$$

using the partial differential equation (PDE) solver tool in Matlab and constant-charge boundary conditions. Here, $U = e\varphi/k_BT$ is the dimensionless local electrostatic potential (φ), $\kappa^{-1} = (2Ce^2/\varepsilon\varepsilon_0 k_BT)$ the Debye length, and a the scaling length (100 nm) within the simulation cell. Further, C is the salt concentration in the solution, ε the dielectric constant of the medium, ε_0 the permittivity of free space, k_B the Boltzmann constant, and T the absolute temperature. The constant-charge boundary condition can be described as $\mathbf{n}\cdot(\Delta U) = e^2/\varepsilon\varepsilon_0 k_BT\sigma_s a$, where $\mathbf{n}$ is the normal to the PMMA surface and σ_s the surface charge density at the PMMA surface. Outside the groove, σ_s was assumed to be 0, and inside the groove, the surface charge density of the PMMA profile was assumed to be $\sigma_s = -75$ nC/cm^2. The surface charge density of the APTES-functionalized groove bottom $\sigma_s = 275$ nC/cm^2 and the nanoparticle $\sigma_P = -187$ nC/cm^2 were calculated using a semiempirical approach[39] based on the ζ-potential. The potential energy $q\Delta U$ of a charge q over the groove was calculated at $y = -50$ nm, where q is the particle charge and ΔU is the potential depth. Here the particles were reduced to point charges with $q = -38e$ (e is the elementary charge). Figure 2a shows the electrostatic potential contribution U for a groove with depth $d = 110$ nm, height $h = 40$ nm, and concentration $C = 5 \times 10^{-4}$ mol/L. It is clearly seen that APTES-functionalized surface is at an energy minimum, whereas the profile of the PMMA is at the energy maximum compared to the PMMA surface or the APTES-functionalized surface. Hence, the minimum energy in the groove facilitates trapping of the nanoparticles. In addition, $q\Delta U$ in the groove is substantially larger than the thermal energy, k_BT, so the particles can be stably trapped. Furthermore, it is noted that the groove width largely affects the electrostatic potential distribution in the 1D grooves. For the same density of the positively charged surface, the wider the groove, the higher the electrostatic potential drop in the groove (Figure 2b), which helps us understand the mechanism for interparticle modulation, as shown in Figure 1d. In other words, the wider the groove, the larger the electrostatic interaction between the nanoparticles and the substrate. Therefore, we can adjust the average interparticle distance of a 1D single-particle array of Au nanoparticles by simply modulating the width of groove on the same chip based on the electrostatic trapping.

Since the interparticle distance plays an important role in the plasmonic properties of nanoparticles,[14] we investigated the surface-enhanced Raman scattering (SERS) behavior of the obtained multiplexed 1D nanoparticle arrays on the substrate. The multiplexed 1D nanoparticle (32 nm) arrays (Figure 3a−c) were functionalized with methylene blue (MB) and subsequently characterized by confocal Raman microscopy. The linear nanoparticle arrays showed dramatic SERS response in their polarization dependence (Figure S1 in the Supporting Information), where the Raman signal for the longitudinal polarization with respect to the long axis of the 1D particle arrays is much stronger than that of the transverse polarization. Therefore, in the following experiment, we focused only on excitation with the longitudinal polarization. The two characteristic peaks (Figure 3d) for MB at 1622 and 1399 cm^{-1} corresponding to C−C stretching and C−N stretching modes were observed.[40] The 1D Au nanoparticle array with the smallest interparticle distance (40 nm, Figure 3c) showed much higher Raman signal compared to that observed from 1D Au particle array with larger interparticle distance (100 nm, Figure 3a, and 66 nm Figure 3b). We employed the peak maximum to estimate the enhancement factor (EF) of 1D Au nanoparticle arrays over pure MB through the following equation:

$$\mathrm{EF} = \frac{I_{\text{array MB}}}{N_{\text{array MB}}} \Big/ \frac{I_{\text{pure MB}}}{N_{\text{pure MB}}} \quad (2)$$

where I is the intensity of the characteristic SERS peak and N is the number of molecules probed. The areas of the 1622 cm^{-1} band were used for determination of the intensity. While determining the number of

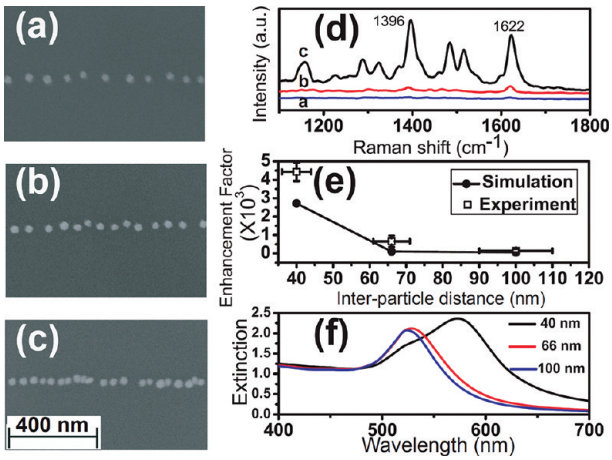

Figure 3. (a−c) SEM images, (d) SERS spectra, (e) experiment and simulation SERS enhancement factor curve under 633 nm irradiation, and (f) electrodynamic modeling calculations for UV−vis extinction spectra of single-particle chains of 32 nm Au nanoparticles with tunable interparticle distance (center to center, from 100 ± 10, 66 ± 5, to 40 ± 4 nm; and the ionic strength of Au nanoparticle solution is 5.0 × 10^{-3} mol/L).

molecules probed, we assumed that the MB molecules were absorbed as a monolayer onto the particle surface of 1D array.[41] $N_{\text{array MB}}$, the number of molecules absorbed onto the particle surface of 1D array probed in the SERS spectrum, is calculated from the following equation:[41]

$$N_{\text{array MB}} = nA_{\text{laser}}A_{\text{N}}/\sigma \quad (3)$$

where n is defined as the particle density of 1D Au particle arrays in the laser spot area, determined by the interparticle distance (center to center) of 1D Au particle arrays. A_{laser} is the area of the laser spot (1 μm^2), A_{N} is the area of single Au nanoparticle, and σ is the area occupied by one MB molecule (0.8 nm^2).[41] On the other hand, the number of measured molecules in the pure MB sample was determined from the following equation:[32]

$$N_{\text{pure MB}} = 6.02 \times 10^{23} \times \rho V/M \quad (4)$$

where ρ is the density of MB, V is the volume (determined by the laser beam size; the collected sample size is roughly 1 μm^3), and M is the molecular weight of MB. On the basis of the calculations in eqs 2−4, EF can be determined. The observed SERS enhancement factor for 1D Au particle array with 40 nm interparticle distance is about 100 times larger than that with 100 nm interparticle distance at 633 nm irradiation wavelength, as shown in Figure 3e.

To clarify the structural basis for the Raman enhancement phenomena associated with interparticle distance, simulation of the UV−vis spectra and local electric fields (E) of 1D nanoparticle arrays (excited at 633 nm) was performed in vacuum using the discrete dipole approximation (DDA) method.[42−44] All of the electrodynamic modeling was done by the DDSCAT7.0 program.[45] In DDA, gold spheres are represented as a cubic array of polarizable elements whose polarizability is determined from the nanoparticle dielectric function.[42,46] Dipoles are induced as a result of the interaction of the polarizable elements with an incident plane wave field and with fields arising from the other polarizable elements. The fields outside the nanoparticle are determined from the superposition of the incident plane wave and the fields of the induced dipoles. These fields are calculated with half grid spacing from the surface, instead of right on the surface, in order to avoid numerical instabilities that arise at the surface. The grid spacing used was 0.5 nm, and the dielectric constants of gold were used from Johnson and Christy.[47] The refractive index of the surrounding medium was fixed at a value of 1.30 to include the substrate effect implicitly. As the interparticle distance decreases, the plasmonic band shifts to higher wavelength (red shift) (see Figure 3f), demonstrating the tunability of the surface plasmon resonance by controlling the interparticle distance based on our strategy. It is found that the magnitude of the calculated enhancement factors ($\int |E|^4 ds$) for the 1D nanoparticle array with the smallest interparticle distance (40 nm) is much larger than other two particle arrays with larger interparticle distance (66 and 100 nm), which are in good agreement with experiments (Figure 3e). One reason for this is that the 1D nanoparticle array with the smallest interparticle distance (40 nm) is closer to resonance at 633 nm than the other two arrays. We further measured the Raman spectra for the above-mentioned 1D Au nanoparticle arrays with difference interparticle distances at 532 nm irradiation wavelength. It was found that these three different arrays had similar Raman intensity, which could be due to the similar resonance for these three nanoparticle arrays at 532 nm (Figure S2 in the Supporting Information).

We further demonstrated that it was possible to fabricate multiplexed 1D nanoparticle arrays with different particle size on the same substrate based upon

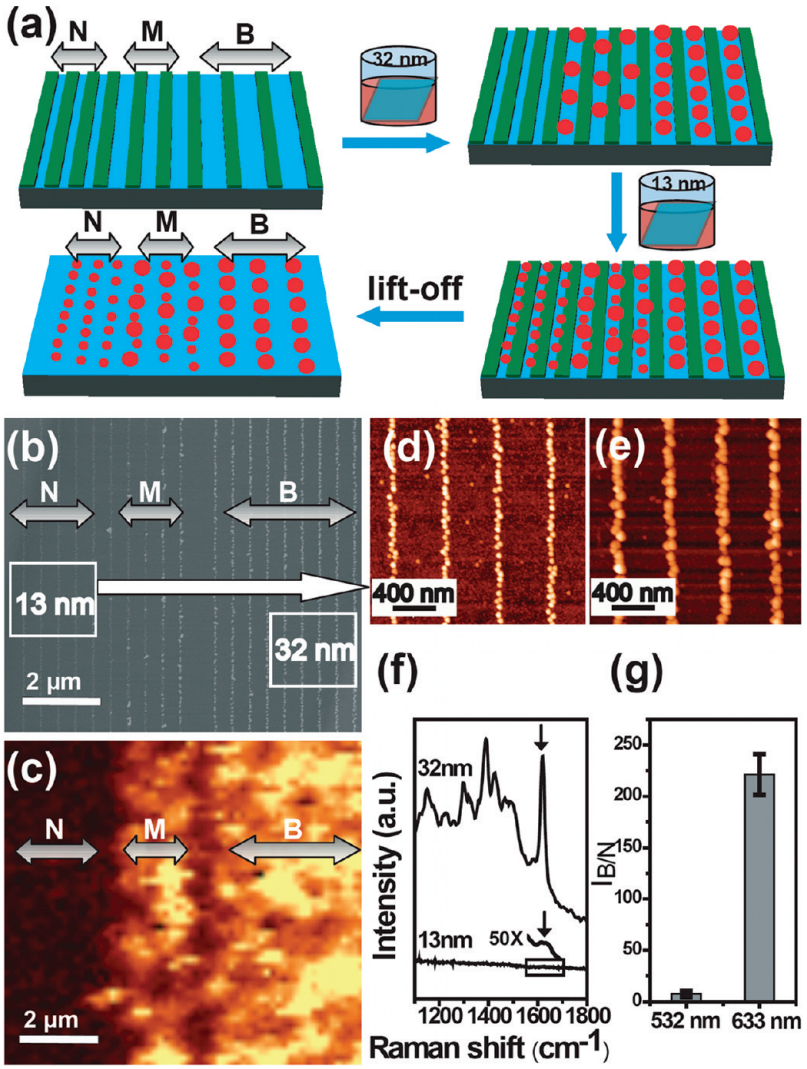

Figure 4. (a) Schematic illustration of fabricating multiplexed 1D nanoparticle arrays with different particle size on the same substrate, (b) SEM image and (c) confocal Raman image of 1D particle array with two different size particles at the desired location on one chip (left side, 13 nm Au array; middle, mixed array of 13 and 32 nm Au nanoparticle in medium grooves; and right side, 32 nm Au nanoparticle array), AFM images of 1D arrays for (d) 13 nm Au nanoparticles and (e) 32 nm Au nanoparticles, (f) SERS spectra for these two different arrays at 633 nm irradiation wavelength, and (g) the peak intensity ratio at 1622 cm^{-1} of broad groove area to narrow groove area ($I_{B/N}$) at 532 and 633 nm irradiation wavelength, respectively.

the concept of spatially modulated electrostatic potential. It is noted that only when the effective diameter of the nanoparticle is smaller than the width of the groove, the nanoparticles can be assembled into the grooves.[20] Therefore, it is envisaged that we could precisely position the different sized Au nanoparticles into the desired location on the same chip by suitably controlling the width of the grooves. As proof-of-concept, we rationally designed a patterned surface with three different width of grooves, 170 nm (broad, B), 130 nm (medium, M), and 100 nm (narrow, N), to build multiplexed 1D nanoparticle arrays with different particle size (Figure 4a). First, we immersed the patterned substrate into the solution with 32 nm Au nanoparticles (the effective diameter of about 102 nm based on the ionic strength of the solution of 7.5×10^{-5} mol/L). Due to the spatial confinement, Au nanoparticles can be only deposited in the broad grooves of 170 with 102 nm interparticle distance (center to center) and in the medium grooves of 130 nm with larger interparticle distance (Figure 4b), but there is no deposition in the narrow grooves of 100 nm, which is smaller than its effective diameter. Then, we immersed the same chip into the solution with 13 nm Au nanoparticles (the effective diameter of about 83 nm based on the ionic strength of the solution being 7.5×10^{-5} mol/L). The Au nanoparticles were deposited into the grooves with 130 and 100 nm in-width grooves, and there is no deposition in the 170 nm grooves since the gap between the particle is 70 nm, which is smaller than the effective diameter of 13 nm Au nanoparticle (83 nm) (Figure 4b). AFM images (Figure 4c,d) further clearly show that 13 nm Au nanoparticles were deposited into the grooves with

100 nm width, while 32 nm Au nanoparticles were deposited into the grooves with 170 nm width. Other methods, such as dip coating,[27] can only fabricate lines of mixed nanoparticles for the different size particles. Our method described above can fabricate distinct lines of different particles. These kinds of multiplexed 1D nanoparticle arrays would be interesting for the multiplexed SERS since the resonance for 1D 32 nm Au nanoparticle arrays is closer to 633 nm compared with that for 1D 13 nm Au nanoparticle arrays. The obtained multiplexed 1D nanoparticle arrays (Figure 4b) were functionalized with MB and subsequently characterized by confocal Raman microscopy (Figure 4e). Figure 4f shows SERS spectra recorded from 1D 32 nm, 1D mixture size, and 13 nm Au nanoparticle arrays. Indeed, 1D 32 nm Au nanoparticle arrays show much higher Raman enhancement compared to the enhancement observed with 1D 13 nm Au nanoparticle arrays. However, when such multiplexed 1D nanoparticle arrays were irradiated with 532 nm laser, the Raman measurement (Figure S3 in the Supporting Information) showed that the relative Raman intensity ratio of the broad area pattern to the narrow area pattern ($I_{B/N}$) was much smaller at 532 nm compared with that at 633 nm, as shown in Figure 4g. These results have shown that we had the preliminary capability to tune the SERS response based on the rational selection of laser for irradiation.

CONCLUSIONS

We demonstrated a synergetic combination of geometry-mediated trapping with electrostatic interaction between nanoparticles and substrate to produce spatially modulated electrostatic potential, which is used to construct 1D multiplexed nanoparticle arrays on one chip. Multiplexed 1D nanoparticle arrays with tunable interparticle distance and/or multiplexed 1D nanoparticle arrays with different particle size on the same substrate were demonstrated. Since the surface plasmon absorption bands can be tuned depending on the interparticle distance or the particle size, we demonstrated a multiplexed SERS response on such a patterned substrate. This strategy provides a general approach for using a colloidal nanoparticle to produce high-quality encoded nanostructures with multiplex 1D periodic nanoparticle arrays in desired locations on one chip, which have potential applications in multiplexed response of surface vibrational spectroscopy, biological and chemical diagnostics, and so on.

METHODS

Amine-functionalized silane (APTES) was fabricated on a Si substrates capped with a 300 nm SiO_2 oxide (SiO_2/Si) by a vacuum vapor method. Cleaned substrates were placed in an air-tight vial, which contained one drop of APTES. The vial was heated at 70 °C for 3 h in a vacuum oven. As a consequence, the APTES molecules are organized in a layer with their free amino groups away from the substrate. The PMMA film of thickness 40 nm was spin-coated as the resist layer, and the 1D groove and hole pattern were generated by EBL to expose the amino-modified SiO_2/Si substrate with different width. The Au nanoparticles were prepared by sodium citrate reduction of $HAuCl_4$ solution.[20] The substrate was then immersed into Au nanoparticle solution for 8−12 h and afterward rinsed by deionized water and dried with the nitrogen. PMMA as the resist layer can be easily removed in acetone by sonication.

E-beam lithography was performed on a LEO VP 1530 field-emission scanning electron microscope with a Raith Elphy Plus lithography attachment system. Atomic force microscopy measurements were carried out on a Multimode Nanoscope IIIa instrument (Digital Instrument) operating in tapping mode with silicon cantilevers (resonance frequency in the range of 280−340 kHz). Raman spectra and images were recorded with a confocal Raman microscope (WiTec Alpha300) equipped with a piezo-scanner and 100× microscope objectives (NA = 0.9). Samples were excited with a He−Ne laser (632.8 nm, Coherent Inc.) with a spot size of ~1 μm. For a typical Raman image with a scan range of 10 μm × 10 μm, complete Raman spectra were acquired on every pixel with an integration time 0.5 s per spectrum and an image resolution of 100 pixels × 100 lines.

Acknowledgment. This work was financially supported by SERC-TSRP (1021520015).

Supporting Information Available: SERS spectra under 0 and 90° orientation relative to laser polarization; details of electrodynamic modeling calculations for UV−vis extinction spectra and local electric fields (E (90°) and E (0°) direction along 1D array); and SERS enhancement measurement for multiplexed 1D nanoparticle arrays at 532 nm irradiation wavelength. This material is available free of charge *via* the Internet at http://pubs.acs.org.

REFERENCES AND NOTES

1. Anker, J. N.; Hall, W. P.; Lyandres, O.; Shah, N. C.; Zhao, J.; Van Duyne, R. P. Biosensing with Plasmonic Nanosensors. *Nat. Mater.* **2008**, *7*, 442–453.
2. Atwater, H. A.; Polman, A. Plasmonics for Improved Photovoltaic Devices. *Nat. Mater.* **2010**, *9*, 205–213.
3. Knight, M. W.; Sobhani, H.; Nordlander, P.; Halas, N. J. Photodetection with Active Optical Antennas. *Science* **2011**, *332*, 702–704.
4. Chen, X. D.; Lenhert, S.; Hirtz, M.; Lu, N.; Fuchs, H.; Chi, L. F. Langmuir−Blodgett Patterning: A Bottom-Up Way To Build Mesostructures over Large Areas. *Acc. Chem. Res.* **2007**, *40*, 393–401.
5. Tao, A.; Sinsermsuksakul, P.; Yang, P. Tunable Plasmonic Lattices of Silver Nanocrystals. *Nat. Nanotechnol.* **2007**, *2*, 435–440.
6. Huang, J. X.; Kim, F.; Tao, A. R.; Connor, S.; Yang, P. D. Spontaneous Formation of Nanoparticle Stripe Patterns through Dewetting. *Nat. Mater.* **2005**, *4*, 896–900.
7. Sharpe, R. B. A.; Burdinski, D.; Huskens, J.; Zandvliet, H. J. W.; Reinhoudt, D. N.; Poelsema, B. Template-Directed Self-Assembly of Alkanethiol Monolayers: Selective Growth on Preexisting Monolayer Edges. *Langmuir* **2007**, *23*, 1141–1146.
8. Daniel, M. C.; Astruc, D. Gold Nanoparticles: Assembly, Supramolecular Chemistry, Quantum-Size-Related Properties, and Applications toward Biology, Catalysis, and Nanotechnology. *Chem. Rev.* **2004**, *104*, 293–346.
9. Burda, C.; Chen, X. B.; Narayanan, R.; El-Sayed, M. A. Chemistry and Properties of Nanocrystals of Different Shapes. *Chem. Rev.* **2005**, *105*, 1025–1102.

10. Mulvihill, M. J.; Ling, X. Y.; Henzie, J.; Yang, P. D. Anisotropic Etching of Silver Nanoparticles for Plasmonic Structures Capable of Single-Particle SERS. *J. Am. Chem. Soc.* **2010**, *132*, 268–274.
11. Fan, J. A.; Wu, C. H.; Bao, K.; Bao, J. M.; Bardhan, R.; Halas, N. J.; Manoharan, V. N.; Nordlander, P.; Shvets, G.; Capasso, F. Self-Assembled Plasmonic Nanoparticle Clusters. *Science* **2010**, *328*, 1135–1138.
12. Fogler, M. M.; Malinin, S. V.; Nattermann, T. Coulomb Blockade and Transport in a Chain of One-Dimensional Quantum Dots. *Phys. Rev. Lett.* **2006**, *97*, 096601.
13. Tang, Z. Y.; Kotov, N. A. One-Dimensional Assemblies of Nanoparticles: Preparation, Properties, and Promise. *Adv. Mater.* **2005**, *17*, 951–962.
14. Wei, Q. H.; Su, K. H.; Durant, S.; Zhang, X. Plasmon Resonance of Finite One-Dimensional Au Nanoparticle Chains. *Nano Lett.* **2004**, *4*, 1067–1071.
15. Ooi, C. H. R.; Yeung, T. C. A.; Lim, T. K.; Kam, C. H. General Electromagnetic Density of Modes for a One-Dimensional Photonic Crystal. *Phys. Rev. E* **2000**, *62*, 7405–7409.
16. Chen, X. D.; Rogach, A. L.; Talapin, D. V.; Fuchs, H.; Chi, L. F. Hierarchical Luminescence Patterning Based on Multiscaled Self-Assembly. *J. Am. Chem. Soc.* **2006**, *128*, 9592–9593.
17. Lopes, W. A.; Jaeger, H. M. Hierarchical Self-Assembly of Metal Nanostructures on Diblock Copolymer Scaffolds. *Nature* **2001**, *414*, 735–738.
18. Zach, M. P.; Ng, K. H.; Penner, R. M. Molybdenum Nanowires by Electrodeposition. *Science* **2000**, *290*, 2120–2123.
19. Demers, L. M.; Ginger, D. S.; Park, S. J.; Li, Z.; Chung, S. W.; Mirkin, C. A. Direct Patterning of Modified Oligonucleotides on Metals and Insulators by Dip-Pen Nanolithography. *Science* **2002**, *296*, 1836–1838.
20. Jiang, L.; Wang, W. C.; Fuchs, H.; Chi, L. F. One-Dimensional Arrangement of Gold Nanoparticles with Tunable Interparticle Distance. *Small* **2009**, *5*, 2819–2822.
21. Spatz, J. P.; Chan, V. Z. H.; Mossmer, S.; Kamm, F. M.; Plettl, A.; Ziemann, P.; Moller, M. A Combined Top-Down/Bottom-Up Approach to the Microscopic Localization of Metallic Nanodots. *Adv. Mater.* **2002**, *14*, 1827–1832.
22. Coskun, U. C.; Mebrahtu, H.; Huang, P. B.; Huang, J.; Sebba, D.; Biasco, A.; Makarovski, A.; Lazarides, A.; LaBean, T. H.; Finkelstein, G. Single-Electron Transistors Made by Chemical Patterning of Silicon Dioxide Substrates and Selective Deposition of Gold Nanoparticles. *Appl. Phys. Lett.* **2008**, *93*, 123101.
23. Lin, H. Y.; Tsai, L. C.; Chen, C. D. Assembly of Nanoparticle Patterns with Single-Particle Resolution Using DNA-Mediated Charge Trapping Technique: Method and Applications. *Adv. Funct. Mater.* **2007**, *17*, 3182–3186.
24. Cui, Y.; Bjork, M. T.; Liddle, J. A.; Sonnichsen, C.; Boussert, B.; Alivisatos, A. P. Integration of Colloidal Nanocrystals into Lithographically Patterned Devices. *Nano Lett.* **2004**, *4*, 1093–1098.
25. Lee, C. S.; Lee, H.; Westervelt, R. M. Microelectromagnets for the Control of Magnetic Nanoparticles. *Appl. Phys. Lett.* **2001**, *79*, 3308–3310.
26. Ray, M. A.; Kim, H.; Jia, L. Dynamic Self-Assembly of Polymer Colloids To Form Linear Patterns. *Langmuir* **2005**, *21*, 4786–4789.
27. Huang, J. X.; Tao, A. R.; Connor, S.; He, R. R.; Yang, P. D. A General Method for Assembling Single Colloidal Particle Lines. *Nano Lett.* **2006**, *6*, 524–529.
28. Vidoni, O.; Reuter, T.; Torma, V.; Meyer-Zaika, W.; Schmid, G. Quasi One-Dimensional Gold Cluster Arrangements. *J. Mater. Chem.* **2001**, *11*, 3188–3190.
29. Rao, C. N. R.; Kulkarni, G. U.; Thomas, P. J.; Edwards, P. P. Metal Nanoparticles and Their Assemblies. *Chem. Soc. Rev.* **2000**, *29*, 27–35.
30. Stebe, K. J.; Lewandowski, E.; Ghosh, M. Oriented Assembly of Metamaterials. *Science* **2009**, *325*, 159–160.
31. Wilson, R.; Cossins, A. R.; Spiller, D. G. Encoded Microcarriers for High-Throughput Multiplexed Detection. *Angew. Chem., Int. Ed.* **2006**, *45*, 6104–6117.
32. Qin, L.; Banholzer, M. J.; Millstone, J. E.; Mirkin, C. A. Nanodisk Codes. *Nano Lett.* **2007**, *7*, 3849–3853.
33. Lundgren, A. O.; Bjorefors, F.; Olofsson, L. G. M.; Elwing, H. Self-Arrangement among Charge-Stabilized Gold Nanoparticles on a Dithiothreitol Reactivated Octanedithiol Monolayer. *Nano Lett.* **2008**, *8*, 3989–3992.
34. Kooij, E. S.; Brouwer, E. A. M.; Wormeester, H.; Poelsema, B. Ionic Strength Mediated Self-Organization of Gold Nanocrystals: An AFM Study. *Langmuir* **2002**, *18*, 7677–7682.
35. Joo, J.; Moon, S.; Jacobson, J. M. Ultrafast Patterning of Nanoparticles by Electrostatic Lithography. *J. Vac. Sci. Technol., B* **2006**, *24*, 3205–3208.
36. Joo, J.; Chow, B. Y.; Jacobson, J. M. Nanoscale Patterning on Insulating Substrates by Critical Energy Electron Beam Lithography. *Nano Lett.* **2006**, *6*, 2021–2025.
37. Thamida, S. K.; Chang, H. C. Nonlinear Electrokinetic Ejection and Entrainment Due to Polarization at Nearly Insulated Wedges. *Phys. Fluids* **2002**, *14*, 4315–4328.
38. Yordanov, V.; Ivanova-Stanik, I.; Blagoev, A. Pic-Mcc Method with Finite Element Solver for Poisson Equation Used in Simulation of the Breakdown Phase in Dense Plasma Focus Devices. In *J. Phys.: Conf. Ser.*; Benova, E., Atanassov, V., Zhelyazkov, I., Eds.; Iop Publishing Ltd.: Bristol, 2006; Vol. 44, pp 215–220.
39. Loeb, A. L.; Wiersma, P. H.; Overbeek, J. T. G. *The Electrical Double Layer around a Spherical Colloidal Particle*; MIT Press: Cambridge, MA, 1961.
40. Nicolai, S. H. A.; Rubim, J. C. Surface-Enhanced Resonance Raman (SERR) Spectra of Methylene Blue Adsorbed on a Silver Electrode. *Langmuir* **2003**, *19*, 4291–4294.
41. Jena, B. K.; Mishra, B. K.; Bohidar, S. Synthesis of Branched Ag Nanoflowers Based on a Bioinspired Technique: Their Surface Enhanced Raman Scattering and Antibacterial Activity. *J. Phys. Chem. C* **2009**, *113*, 14753–14758.
42. Draine, B. T.; Flatau, P. J. Discrete-Dipole Approximation for Periodic Targets: Theory and Tests. *J. Opt. Soc. Am. A* **2008**, *25*, 2693–2703.
43. Li, S. Z.; Pedano, M. L.; Chang, S. H.; Mirkin, C. A.; Schatz, G. C. Gap Structure Effects on Surface-Enhanced Raman Scattering Intensities for Gold Gapped Rods. *Nano Lett.* **2010**, *10*, 1722–1727.
44. Chen, X. D.; Li, S. Z.; Xue, C.; Banholzer, M. J.; Schatz, G. C.; Mirkin, C. A. Plasmonic Focusing in Rod-Sheath Heteronanostructure. *ACS Nano* **2009**, *3*, 87–92.
45. Draine, B. T.; Flatau, P. J. *User Guide for the Discrete Dipole Approximation Code Ddscat 7.0*. **2008**, DOI: arxiv/0809.0337.
46. Draine, B. T.; Flatau, P. J. Discrete-Dipole Approximation for Scattering Calculations. *J. Opt. Soc. Am. A* **1994**, *11*, 1491–1499.
47. Johnson, P. B.; Christy, R. W. Optical-Constants of Noble-Metals. *Phys. Rev. B* **1972**, *6*, 4370–4379.